Chemical Engineering Journal 531 (2026) 174182

Contents lists available at ScienceDirect

Chemical Engineering Journal

journal homepage: www.elsevier.com/locate/cej

Combined photocatalysis and solar distillation: Promoting synergistic effects for a more efficient VOC/SVOC rejection☆

Hady Hamza [a], Marco L.P. Schiavoni [a], Begüm Aksu [b], Abdul Basit Shah Syed [c], Vanni Lughi [c], Maria Vittoria Diamanti [b], Daniela Meroni [a,d,*]

[a] Department of Chemistry, Università degli Studi di Milano, Milan, Italy
[b] Department of Chemistry, Materials and Chemical Engineering "Giulio Natta", Politecnico di Milano, Milan, Italy
[c] Department of Engineering and Architecture, Università degli studi di Trieste, Trieste, Italy
[d] Consorzio INSTM, Florence, Italy

ARTICLE INFO

Keywords:
Volatile organic compounds
Interfacial distillation
Pollutant rejection
Photocatalysis
Wastewater treatment
Photothermal evaporator

ABSTRACT

Photocatalytic-photothermal evaporators are emerging as promising water purification technologies capable of removing both inorganic and organic pollutants while offering low-cost and low-energy desalination. Despite their potential, the interplay between photocatalysis and photothermal evaporation remains poorly understood. Here, we investigate the sequential application of the two processes and demonstrate, for the first time, the existence of synergistic effects that are independent of the specific materials used. We show that pollutant rejection by evaporation is very effective on the aromatic intermediates formed via hydroxyl-radical attack – an insight of general relevance to advanced oxidation processes. However, we also identify p-benzoquinone as a critical volatile intermediate whose concentration remains significant in the distillate after conventional liquid-phase photocatalysis combined with evaporation. By examining the role of the water matrix, including common inorganic electrolytes and non-volatile organic compounds, we further reveal conditions under which the combined process becomes practically ineffective – an issue not previously recognized for photocatalytic–photothermal systems. Building on these findings, we propose an improved treatment sequence in which the evaporation step is brought forward, mitigating the inhibitory effects of non-volatile species and enabling robust synergistic coupling. This work highlights the overlooked importance of gas-phase photocatalysis and provides a rational framework for the future design and optimization of photocatalytic-photothermal evaporators.

1. Introduction

Approximately 3.2 billion people live in regions facing moderate to severe water shortages [1]. The worsening impacts of climate change, seawater intrusion, and environmental pollution are further intensifying this crisis. Desalination offers a reliable, non-conventional source of water, alleviating pressure on existing freshwater supplies. Around 16,000 desalination plants operate worldwide, providing water to more than 300 million people [2]. However, commonly used techniques, such as thermal desalination and reverse osmosis, are highly energy intensive [3,4]. Therefore, developing energy-efficient technologies capable of converting wastewater, seawater, or brackish water into potable water has become an urgent priority.

Solar-driven interfacial evaporators have emerged as a promising low-energy and cost-effective solution. These systems harness solar energy to generate heat, accelerating the evaporation of water; the resulting vapor is then condensed in solar stills to yield purified water [5]. Solar evaporators can provide clean water in disaster areas thanks to their off-grid capability, offer a low-energy solution to upgrade the quality of saline and polluted water, and can combine water purification with energy generation and evaporative cooling [6,7]. These features position this technology within the broader framework of climate-change adaptation solutions [8].

Since 2016, solar distillation has gained renewed attention thanks to evaporators based on interfacial heating [9]. These designs localize solar-thermal conversion at the evaporating interface while keeping the

☆ This article is part of a Special issue entitled: 'EAAOP-7' published in Chemical Engineering Journal.

* Corresponding author at: Department of Chemistry, Università degli Studi di Milano, Milan, Italy.
E-mail address: daniela.meroni@unimi.it (D. Meroni).

https://doi.org/10.1016/j.cej.2026.174182
Received 29 November 2025; Received in revised form 30 January 2026; Accepted 13 February 2026
Available online 13 February 2026

bulk water cooler, thereby reducing heat loss and improving efficiency. Typically, a photothermal absorber with high solar absorption and conversion efficiency is embedded within a porous, hydrophilic support that provides floatation and thermal insulation [10]. Despite recent progress, the technology is still in its early stages. Numerous designs and materials have been explored, yet no definitive optimal configuration has been identified [11,12]. Among the recognized issues, the inefficient removal of volatile and semi-volatile contaminants can compromise water quality [13]. To solve this issue, the incorporation of photocatalytic materials into solar-driven interfacial evaporators has recently emerged as a promising approach [14]. Photocatalysis is indeed a well-known advanced oxidation process, able to degrade a broad range of recalcitrant pollutants [15,16]. Overall, many of the characteristics required for efficient photothermal materials align with those needed for floating solar-photocatalytic materials, facilitating the integration of these two technologies [17]. This dual-function strategy enables the simultaneous removal of inorganic and organic contaminants while operating with substantially lower energy input and maintaining long-term performance [18–20].

Nevertheless, several open questions remain. This combined approach is very complex, as photocatalytic oxidation and photothermal evaporation act simultaneously and may interact synergistically. However, the way these two processes influence each other is still poorly explored in the literature [21], and potential intrinsic limitations of the combined approach remain largely unaddressed.

Among the main potential obstacles, inorganic electrolytes, such as chlorides and bicarbonates, are known to negatively affect the photocatalytic performance of various photocatalytic materials, including TiO_2 [22,23]. Since solar-driven interfacial evaporators are designed to treat highly saline feeds such as seawater, the interactions between water-matrix electrolytes and the photocatalyst in photocatalytic-photothermal evaporators must be systematically investigated. Another important aspect concerns the lack of selectivity of photocatalysis toward organic contaminants: non-volatile species present in the water matrix can slow down the photocatalytic degradation of volatile organic compounds (VOCs), which are the main concern in photothermal evaporators [24]. Finally, it is well known that advanced oxidation processes, such as photocatalysis, can lead to accumulation of degradation byproducts, some of which have similar or even higher toxicity than the parent compound [25,26]: For instance, in the case of phenol—a VOC pollutant—some of its main degradation intermediates, such as p-benzoquinone and hydroquinone, are more toxic than phenol itself [27,28]. Most of the literature on photocatalytic-photothermal evaporators focuses only on the parent compound, neglecting to investigate the fate of the degradation intermediates.

In this context, the present study aims to bridge these gaps, which are crucial for the real-life applicability of photocatalytic-photothermal evaporators. Here, we report for the first time synergistic and antagonistic effects arising during the sequential combination of solar distillation and photocatalytic processes. While less investigated than synergisms in composite materials, synergistic effects can occur also between sequential treatments. Disentangling the various contributions involved has guided us toward the design of a more efficient combined system, showing better performance in challenging conditions such as high salt content and highly polluted matrices.

2. Materials and methods

All chemicals were purchased from Sigma-Aldrich with reagent-grade purity and used as received; doubly distilled water passed through a Milli-Q apparatus was utilized.

2.1. Photocatalyst preparation

The adopted photocatalysts were self-assembled TiO_2 nanotubular arrays, prepared according to a previously reported procedure [29]. In brief, commercially pure ASTM grade 2 titanium meshes ($15 \times 5 \times 0.5$ cm^3) were first cleaned by ultrasonic treatment in ethanol for 10 min. The samples were then anodized under potentiostatic conditions (45 V for 30 min, Potentiostat LTC-Caoduro) in an electrolyte consisting of ethylene glycol $+0.2$ m $NH_4F + 2$ m H_2O. After the anodization step, the meshes were rinsed thoroughly with deionized water, dried under a stream of air, and finally annealed at 500 °C for 2 h to crystallize the initially amorphous oxide layers. The morphology of the photocatalytic layer was analyzed via field-emission Scanning Electron Microscopy (FESEM) on an EVO 50VP microscope (Carl Zeiss AG), after gold sputtering. X-ray diffraction (XRD) patterns were measured on a Philips diffractometer equipped with a PW 1830 generator and PW 1820 vertical goniometer, working in Bragg-Brentano configuration, and using Cu Kα radiation.

2.2. Selected pollutants and test conditions

All tests (evaporation, photocatalytic and combined tests) were carried out on aqueous solutions of two main contaminants: Phenol was selected as model VOC pollutant, while methyl orange (MO) was used as model of a non-volatile organic pollutant. Evaporation tests were also carried out on the main degradation intermediates of phenol (hydroquinone, *p*-benzoquinone, pyrocatechol). Tests were carried out on aqueous solutions of either single contaminants or pollutant binary mixtures. For each pollutant, an initial concentration of 50 mg/L was always adopted to promote accumulation of intermediates and study their fate. Pollutant solutions were prepared in either ultrapure water or in simulated seawater (35 g/L NaCl): both are widely adopted test conditions for photothermal devices [30].

2.3. Pollutant rejection in evaporation tests

A first set of experiments was conducted in a lab-made solar still, entirely made of borosilicate glass, with planar cover. Each test was carried out on an 80 mL aqueous solution of different pollutants, as described in Section 2.2. To avoid confounding effects due to adsorption, no photothermal catalyst was added. Light irradiation of the pollutant solution was performed from the side using an IR lamp (Osram, 250 W thermal lamp, effective power density 75 mW cm^{-2} measured by a Thorlabs S314C thermal power sensor) to promote evaporation. The temperature at the liquid surface was monitored by a thermal camera (FLIR TG267); during tests, a temperature of (40 ± 2)°C was reached when equilibrium conditions were established. Additional tests were also carried out heating the liquid at 50 °C with a hot plate instead of a lamp, to check for any possible photolysis pathways. With the same setup, tests to evaluate dark adsorption by the photocatalyst were carried out by placing the photocatalyst within the solar still over the liquid. The condensed distillate was collected at regular time intervals and analyzed as explained in Section 2.6. Pollutant reject results are reported in terms of distillate concentration ratio (R_D), calculated using Eq. (1):

$$R_D = C_{dist}/C_0 \quad (1)$$

where C_{dist} is the pollutant concentration in the distillate and C_0 is the initial concentration of the pollutant solution [31]. In the present case, R_D values refer to equilibrium conditions (Fig. S1a). The composition of the remaining liquid was also analyzed. Reproducibility was ensured by repeating tests in triplicate.

2.4. Photocatalytic tests in liquid phase

Photocatalytic tests were performed in a 100 mL closed Pyrex jacketed reactor at 25 °C and at spontaneous pH (close to 6 in all tested conditions). Tests were carried out on aqueous solutions of different pollutants as described in Section 2.2. Aerated conditions were ensured

by O_2 bubbling: any volatile species stripped by O_2 bubbling were collected in a low temperature trap and quantified. Before the photocatalytic test, the photocatalyst net was irradiated on both sides with UV light for 60 min to ensure a clean oxide surface. Then, the photocatalyst was immersed in the phenol solution and the system was vigorously stirred in the dark until the adsorption-desorption equilibrium was reached (30 min). Dark adsorption tests showed less than 5% removal for both phenol and MO in the tested conditions. At this point, UV irradiation by a medium pressure metal halide UV lamp (Jelosil HG500 filtered for $\lambda < 320$ nm, effective power density 30 mW cm^{-2} in the 320–400 nm range measured by UVmeter, Delta Ohm HD2302.0 with UV sensitive sensor) was started. The solution was sampled with a syringe at regular time intervals and analyzed according to the procedure reported in Section 2.6.

2.5. Combined tests

A first set of combined experiments were carried out performing sequentially a photocatalytic step in liquid phase (according to the procedure reported in Section 2.3) followed by an evaporation step on the photocatalytically treated solution (according to the procedure reported in Section 2.2). Different tests were performed varying the duration of the photocatalytic step (up to 8 h). In the following, this approach will be called LP-combined test.

A second set of combined experiments were instead performed by photocatalysis on the vapor phase produced by evaporation in the solar still. These tests were carried out in the setup described in Section 2.2, modified by the addition of the photocatalyst net suspended 1 cm above the surface of the pollutant solution. Additional UV irradiation was provided to activate photocatalysis. This approach will be called GP-combined test.

The two setups are schematized in Fig. S2.

2.6. Analytical methods

The treated solution and the distillate from all remediation tests were collected at regular time intervals and monitored by a combination of analytical techniques to determine both the main pollutant concentration and its intermediates. UV–vis spectra were collected on a Shimadzu UV-2600 spectrophotometer in the 200–800 nm range. High-performance liquid chromatography (HPLC) measurements were performed on a Jasco Series 4000 system equipped with a diode-array detector (DAD). Chromatographic separation was performed on a Kinetex C18 column (5 μm, 100 Å, 150 × 4.6 mm) maintained at 30 °C. The detection wavelengths were set at 250, 280 nm and 290 nm. The mobile phases consisted of Phase A: water containing 1% formic acid (v/v), and Phase B: methanol. The analysis was carried out at a constant flow rate of 1.0 mL min^{-1} using the gradient program reported in Table S1. Quantification was performed based on external calibration curves constructed for each compound. Gas chromatography (GC) measurements were carried out using an Agilent 6890 system equipped with a ZB-5 capillary column (Zebron, Phenomenex; 60 m × 0.32 mm i.d., film thickness 1.0 μm). Helium was used as the carrier gas. The oven temperature program was as follows: initial temperature of 120 °C held for 3 min, followed by an increase at 10 °C min^{-1} up to 150 °C, then ramped at 20 °C min^{-1} to a final temperature of 280 °C, which was maintained for 5 min. Analytes were identified based on retention times of authentic standards and quantified using external calibration curves.

Mineralization was studied by total organic carbon (TOC) measurements, measured using a Shimadzu TOC-V CPN Analyzer. The TOC abatement was calculated from the TOC value of the starting solution (TOC_0) and the final TOC value (TOC_t) according to Eq. (2):

$$TOC\ abatement\% = \frac{TOC_0 - TOC_t}{TOC_0} \times 100 \quad (2)$$

The surface of the photocatalyst was analyzed before and after use by Fourier transform infrared (FTIR) spectroscopy in attenuated total reflection (ATR mode) on a PerkinElmer Spectrum 100 spectrophotometer equipped with a single-bounce diamond crystal with a 45° incidence angle.

3. Results and discussion

3.1. Role of electrolytes

Anodization of titanium was chosen as the photocatalyst preparation method due to its ability to produce highly stable immobilized photocatalytic materials [29,32], reducing the risk of the photocatalyst powder being released into the liquid phase during experiments. The TiO_2 layer, upon annealing, becomes crystalline and consists of anatase. Moreover, the choice of TiO_2 – which only activates under UV light, given a band gap of 3.2 eV – further helps prevent photocatalytic pathways during the subsequent evaporation step, as any released photocatalyst powder could not be activated by the lamp used in the evaporation step. Representative FESEM images of the photocatalyst are reported in Fig. 1: the nanotubular structure is clearly appreciable in the top view images, with an average nanotube length of 6 μm. The porous morphology yields a specific surface area of 38 $m^2\ g^{-1}$ [29].

Photocatalytic tests of phenol were carried out under UV irradiation. The pollutant removal follows a pseudo-zero order kinetics (Fig. S4a,b), as expected due to the immobilized nature of the photocatalyst and high phenol concentration. The disappearance rates are reported in Table 1.

While providing a comprehensive investigation of environmental parameter effects on photocatalysis is beyond the scope of this work, the impact of the most relevant factors for the practical application of photothermal evaporators, namely salinity and the presence of non-volatile but oxidizable species, were here investigated. In particular, the effect of concentrated electrolytes was investigated in tests using a 3.5% NaCl aqueous solution as matrix. The presence of high concentrations of electrolytes is known to have marked effects on the volatility and solubility of compounds, surface adsorption and radical generation during photocatalysis. Unsurprisingly, photocatalytic tests of phenol degradation in simulated seawater exhibited a marked drop in the reaction rate (Table 1 and Fig. S4). Chlorides are known to act as radical scavenger in photocatalysis, often leading to a loss of activity of TiO_2 photocatalysts [22].

After the photocatalytic step, the solution was subjected to an evaporation step (LP-combined tests). Different tests were performed varying the duration of the photocatalytic step. The results, in terms of phenol concentration in the collected distillate, $C_{dist.}$ normalized over its initial concentration, C_0, are summarized in Fig. 2a.

The phenol content in the distillate depends on the duration of the photocatalytic step, showing – for tests in ultrapure water – a clear decreasing trend as a function of UV irradiation time. If phenol concentration in the distillate is normalized over the phenol concentration in the solution after the photocatalytic step, $C_{pc,}$ the trend flattens and becomes independent of the UV irradiation time (Fig. 2b). Indeed, the C_{dist} / C_{pc} values are close to the R_D value, calculated from evaporation tests without photocatalytic step. As expected, in these conditions, the lowered concentration of phenol in the distillate reflects the lower phenol concentration in the solution due to photocatalytic oxidation.

The presence of the concentrated electrolyte has a detrimental effect also during LP-combined tests (Fig. 2a): overall phenol concentrations in the distillate are higher than in tests with ultrapure water and display an almost negligible effect of the time of UV light irradiation during the photocatalytic step. Fig. 2b shows the trend of phenol concentration in the distillate normalized over the phenol concentration in the solution after the photocatalytic step, $C_{pc,}$: the C_{dist} / C_{pc} values are close to the R_D value of evaporation tests in simulated seawater, which are larger than the R_D values in ultrapure water [13]. Indeed, Fig. 3a shows invariably larger R_D values in tests with simulated seawater compared to ultrapure water, both for phenol and its degradation intermediates. This

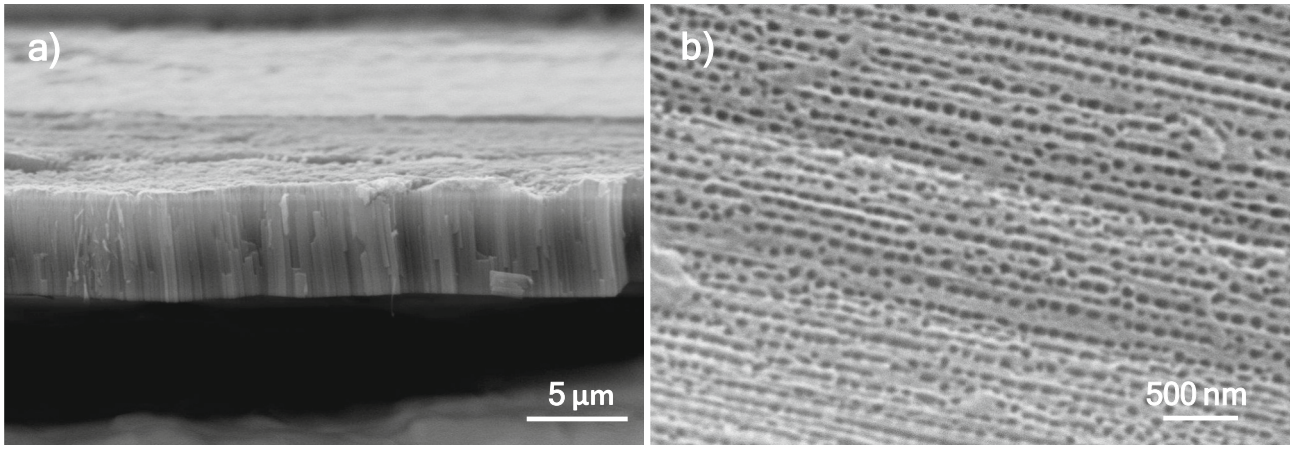

Fig. 1. FESEM images of the TiO_2 nanotubular arrays used as photocatalyst: a) cross-section; b) top view.

Table 1
Pseudo-zero order rate constants of phenol and MO degradation during photocatalytic tests in ultrapure water and simulated seawater. Values of tests performed with a single pollutant are compared with values performed with a mixture of the two pollutants.

		k x 10^5 (mol L^{-1} h^{-1})	
		Ultrapure water	Simulated seawater
Tests with single pollutant	Phenol	3.54 ± 0.06	1.30 ± 0.01
	MO	0.97 ± 0.05	0.14 ± 0.01
Pollutant mixtures	Phenol	1.33 ± 0.09	0.95 ± 0.04
	MO	0.43 ± 0.04	0.01 ± 0.01

observation can be explained by the salting out effect, which leads also to a larger fraction of phenol in the gas phase (Fig. S1b).

The combined effect of the two treatments can be evaluated considering the synergy index, *SI*, a statistical metric to quantify the interaction between two factors, which was calculated according to Eq. (3):

$$SI = \frac{1 - C_t^{comb}/C_0}{1 - (C_t^{PC}/C_0)(C_t^{ET}/C_0)} \quad (3)$$

where C_t^{comb} is the equilibrium concentration of the pollutant in the distilled phase after a combined treatment, C_t^{PC} is the concentration of the pollutant in the solution after the photocatalytic step (with same irradiation time of the combined treatment), and C_t^{ET} is the equilibrium concentration of the pollutant in the distilled phase in tests without photocatalytic step. If *SI* value = 1 the two treatments have independent/additive effect, while $SI > 1$ indicates synergistic effects, i.e. the combined treatment removes more than the independent expectation, i.e. the sum of each individual step independently performed, and $SI < 1$ indicates antagonistic effects. *SI* values are listed in Table 2. Phenol removal by an LP-combined treatment shows a *SI* close to 1, supporting merely additive effects between photocatalysis and pollutant rejection by evaporation, in agreement with conclusions based on C_{dist}/C_{pc} trends.

3.2. Effect of degradation intermediates

The photocatalytic degradation of phenol is a multi-step process, involving several intermediate aromatic and aliphatic compounds before complete mineralization. Early in the process, •OH radical attack of the benzene ring induces the formation of dihydroxylated intermediates, such as catechol and hydroquinone, and their oxidized form, benzoquinone [33–35]. These intermediates are seldom investigated in photocatalytic photothermal evaporators, even though their formation often results in a temporary increase in toxicity of the treated solution and as they are volatile and semivolatile compounds. To clarify

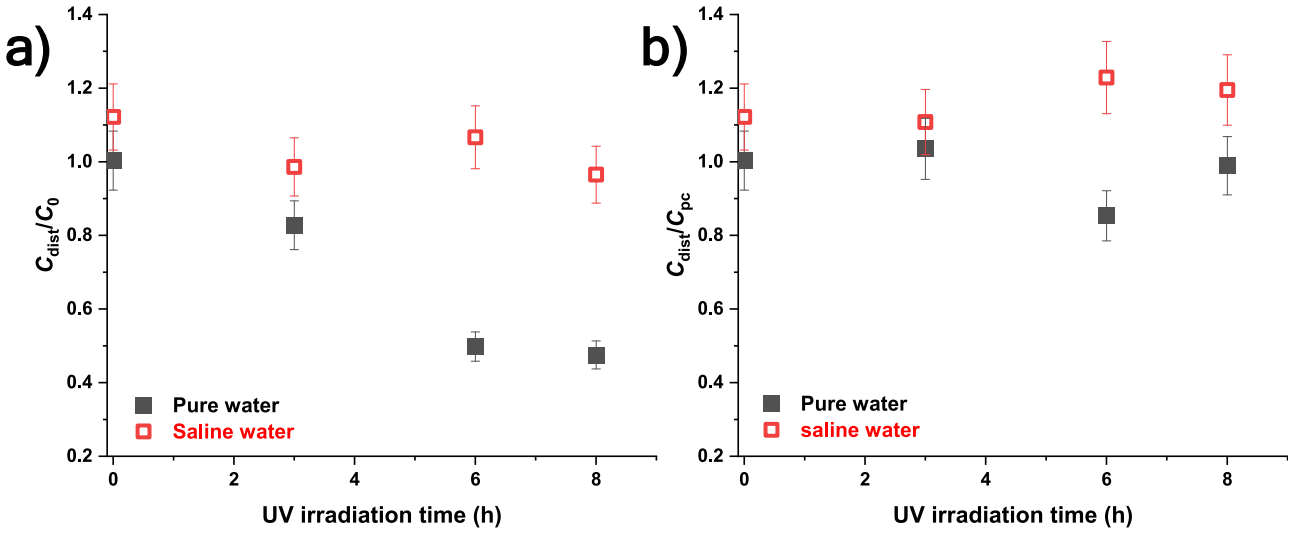

Fig. 2. LP-combined test of a single pollutant in ultrapure water and simulated seawater: a) phenol concentration in the distillate, C_{dist}, normalized for the starting phenol concentration (C_0 = 50 mg/L); b) phenol concentration in the distillate normalized for the phenol concentration after the photocatalytic step, C_{pc}.

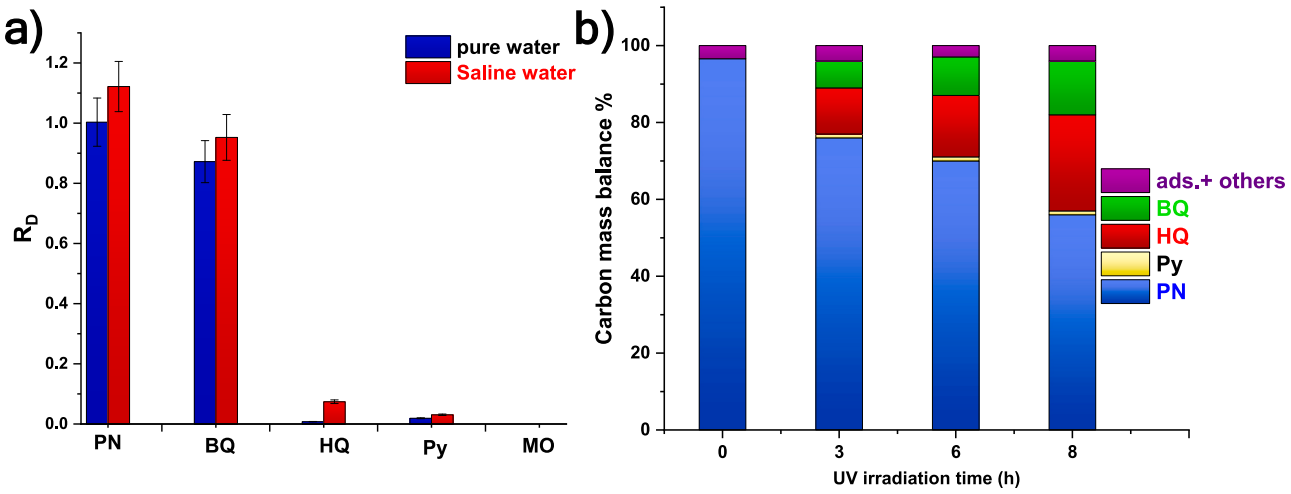

Fig. 3. a) R_D values from evaporation tests of different pollutants (phenol, PN; *p*-benzoquinone, BQ; hydroquinone, HQ; pyrocatechol, Py; methyl orange, MO) in both ultrapure water and in simulated seawater; b) carbon mass balance during photocatalytic tests of phenol in ultrapure water as a function of irradiation time.

Table 2
Synergy index for phenol abatement in combined tests (8 h UV irradiation) calculated according to Eq. (2).

		Synergy Index (*SI*)	
		Ultrapure water	Simulated seawater
LP-combined tests	Single pollutant	1.01	1.09
	Mixture	1.15	0.75
GP-combined tests	Single pollutant	0.90	3.41
	Mixture	1.92	2.11

their fate, evaporation tests were carried out on several of the well-known degradation products of phenol. Results are reported in Fig. 3a and compared with the R_D value of phenol.

As expected from previous tests, phenol is not rejected by sole evaporation, accumulating in the distillate. Benzoquinone shows potential of accumulation in the distillate similar to that of phenol. This is noteworthy as benzoquinone has higher toxicity than phenol itself [27]. Conversely, dihydroxybenzene intermediates are almost completely rejected by evaporation, which can be explained considering their lower volatility [13].

Photocatalytic runs show a progressive accumulation of intermediate molecules in the solution (Fig. 3b), more marked for dihydroxybenzene species. The presence of intermediates is also clearly appreciable from UV–vis spectra of the treated solution (Fig. S5), showing shoulders at longer and shorter wavelengths compared to the phenol peak (λ_{max} = 270 nm). It should be noted that hydroquinone has a main peak at 290 nm, while benzoquinone has one at 240 nm. Fig. S5 shows clearly that, upon evaporation test, the relative content of these species changes. In particular, the shoulder at longer wavelengths decreases in absorbance, whereas the component at shorter wavelengths remains intense. A more quantitative comparison of the intermediates accumulated in the distillate can be made using the Synergy Score, *SS*. To calculate this parameter, we adopted an approach derived from the Bliss Independence model, to take into account that the two treatments act independently:

$$SS = \left(\frac{C_t^{PC}}{C_0} + \frac{C_t^{ET}}{C_0} - \frac{C_t^{PC}}{C_0} \bullet \frac{C_t^{ET}}{C_0}\right) - \frac{C_t^{comb}}{C_0} \quad (4)$$

where C_t^{comb} is the equilibrium concentration of the intermediate in the distillate after the combined treatment of a phenol solution, C_t^{PC} is the concentration of the intermediate in the solution after the photocatalytic step (with same irradiation time of the combined treatment), C_t^{ET} is the equilibrium concentration of the intermediate in the distillate after a evaporation tests of a phenol solution (without photocatalytic step), and C_0 is the initial phenol concentration. According to Eq. (3), if *SS* value = 0 the two treatments have additive effect on the intermediate removal, while $SS > 0$ indicates synergism in the intermediate removal, i.e. there is less accumulation than expected, and $SS < 0$ indicates antagonistic effects, i.e. more accumulation than expected. *SS* values are listed in Table 3.

LP-combined test shows synergistic effects in the removal of hydroquinone, due to the positive interaction between photocatalytic oxidation, where hydroquinone is one of the main intermediates, and its effective rejection by evaporation. This is notable due to the toxicity profile of hydroquinone [28]. To the authors' best knowledge, this synergistic effect of photocatalysis and photothermal evaporation has never been previously recognized. Considering the very low R_D values of other intermediates of phenol degradation (such as pyrocatechol), we can conclude that this synergistic action extends to other intermediate species, in particular to those derived from •OH attack to the ring.

However, there are exceptions, such as p-benzoquinone, which shows an R_D value closer to that of phenol and, consequently, displays accumulation in the distillate, as also reflected by slightly negative SS values. This result is noteworthy not only because of the inherent toxicity of p-benzoquinone [27], but also because it is a commonly identified refractory intermediate in the degradation of a wide variety of aromatic pollutants, and it tends to accumulated in the system [36].

It should be noted that synergy can occur also between two processes that are sequential or temporally/spatially separated. In this case, the observed synergy effects often depend on the order of the treatments, with some combinations leading to synergy and others to merely additive effects [37]. Additive treatments instead are typically independent from the order of application. In our study, the calculated synergy indexes and synergy scores quantitatively support the occurrence of synergistic effects under certain conditions. To further support this conclusion, the synergy scores of the LP-combined test were compared with those from a test performed with same setup but reversed order of the treatments (first evaporation, then liquid phase photocatalysis, keeping constant the ratio between the irradiated photocatalyst area and liquid volume): the latter test showed a synergy score for hydroquinone of 0.03, supporting merely additive effects in this case, compared to the ca. 0.3 of LP-combined test. The difference in the synergy scores depending on the order of the treatments further supports the occurrence of synergistic effects in the removal of hydroxylated intermediates in LP-combined tests.

3.3. Effect of competing non-volatile organics

Natural water matrices are usually very complex and numerous organic species, susceptible to photocatalytic oxidation, are often present. Here a simple mixture composed of phenol, as model VOC, and methyl orange, as a model of a non-volatile pollutant, is investigated. Indeed, the R_D value of methyl orange is negligible, both for tests in ultrapure water and simulated seawater (Fig. 3a).

Table 1 shows that mixing the two pollutants causes a sharp decrease in the reaction rate of photocatalytic degradation of both phenol and methyl orange. This observation can be explained by consumption of reactive radicals and adsorption competition [38].

A detrimental effect of the pollutant mixture is observed also in LP-combined tests (Fig. 4), where phenol concentrations in the distillate are higher than in tests with the single pollutant, and display an almost negligible effect of the time of UV light irradiation during the photocatalytic step. C_{dist} / C_{pc} values are comparable to tests with a single pollutant, indicating a minor effect of MO addition (at the investigated concentration) on phenol R_D values.

LP-combined tests of mixed pollutants in simulated seawater (Fig. S6) show results in line with previous observations. The combination of a hindered photocatalytic degradation and promoted phenol volatility due to salting-out effect leads to phenol concentrations in the distillate consistently above the initial phenol concentration in the liquid phase.

3.4. Role of liquid-phase vs. gas-phase photocatalysis

While the LP-combined approach shows additive and even synergistic effects in terms of the rejection of phenol and its degradation intermediates in simple water matrices, more challenging water matrices lead to unsatisfactory performance between photocatalysis and evaporation. The lowered performances are a direct result of hindered photocatalytic performance caused by competition for adsorption/reactive radicals between the volatile pollutant and interferent, non-volatile species (either organic molecules or inorganic electrolytes). Thanks to this deeper understanding of the process, an alternative setup can be proposed to overcome these issues. The GP-combined approach does not involve any direct contact between the pollutant solution and the photocatalyst. Hence, in this setup, photocatalytic reactions can involve only species in the gas phase, i.e. the volatile components in the wastewater solution that evaporate more easily.

Fig. 5 compares the performance of LP- and GP-combined approaches in terms of C_{dist} / C_0 as a function of the photocatalysis duration.

Fig. 5a clearly shows opposite trends for the two approaches, with LP-combined tests exhibiting the already-described decreasing trend of C_{dist} / C_0 which mirrors the phenol concentration in the solution. Conversely, GP-combined tests show very low C_{dist} values at short UV irradiation time, then the value increases and seems to reach a plateau at values close to those of LP-combined tests after 8 h UV irradiation. The low C_{dist} values observed at short UV irradiation time could reflect insufficient time for equilibration of the system. However, later values clearly are much lower than those of conventional evaporation tests (that have R_D close to 1); the plateau values are very close to those of the LP-combined approach, despite the higher phenol concentration in the liquid basin. This supports the occurrence of photocatalytic degradation of phenol vapours, which is as effective as the LP-combined approach in these operating conditions. It should be noted that dark adsorption tests carried out in the GP-combined test configuration (i.e. with the photocatalyst over the liquid surface) using a starting solution of phenol in ultrapure water showed, after 8 h, negligible adsorption at the photocatalyst surface, as carbon mass balance distribution was almost unvaried compared to tests without photocatalyst. SI values reported in Table 2 also supports this conclusion, showing similar values for LP- and GP-combined approaches for tests with single pollutant in ultrapure water. Notably, SS values, reported in Table 3, support a lower accumulation of all types of intermediates in the distilled phase compared to LP-combined tests. These results are also supported by TOC values (Table S2), showing that the GP-combined test leads to a higher TOC abatement in the distillate compared to the LP-combined test.

The advantage of the GP-combined approach becomes more apparent when more challenging water matrices are tested. Fig. 5b shows that, while phenol concentrations in the distillate during LP-combined tests remained high regardless of the duration of UV irradiation, GP-combined tests exhibited much lower phenol accumulation in the distillate throughout the experiment. The slightly higher C_{dist} / C_0 values observed in GP-tests performed in simulated seawater compared to those in ultrapure water can be attributed to the increased phenol content in the gas phase resulting from the salting-out effect (Fig. S1b). More notably, while the *SI* value of LP-combined approach is close to 1 (Table 2), indicative of mere additivity of the two treatments, the relative value for GP-combined method is $>>1$, supporting highly synergistic effects. Indeed, photocatalysis proceeds in the gas phase unimpeded by the detrimental role of chlorides and abating the phenol content already in the vapor phase. Similar conclusions can be drawn

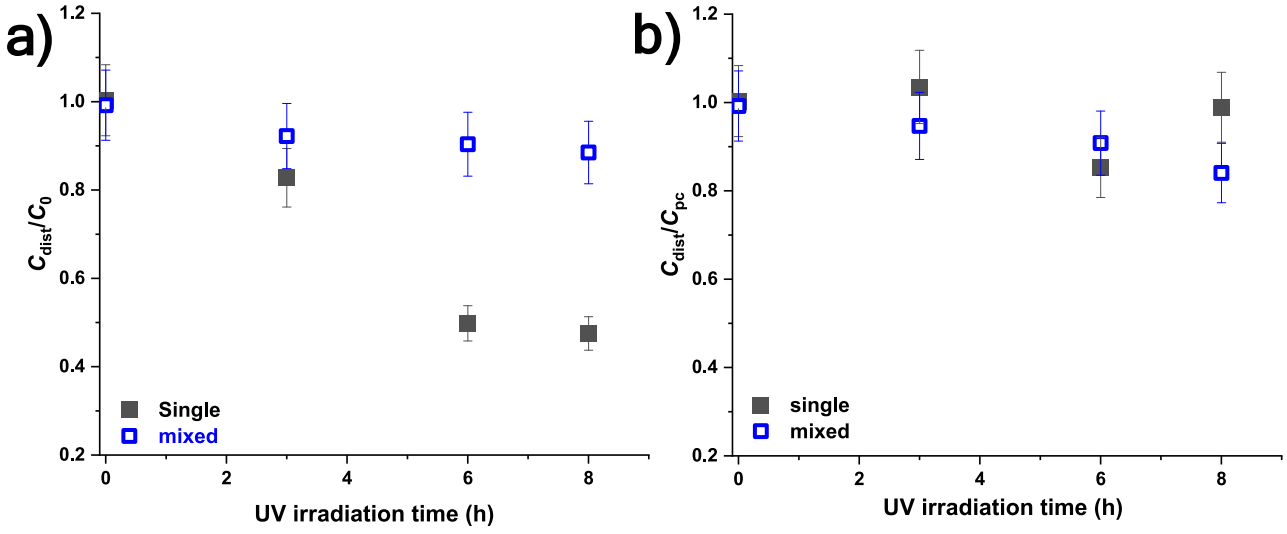

Fig. 4. LP-combined test on a phenol only (single pollutant) and in mixture with MO: a) phenol concentration in the distillate, C_{dist}, normalized for the starting phenol concentration, C_0; b) phenol concentration in the distillate normalized for the phenol concentration after the photocatalytic step, C_{pc}.

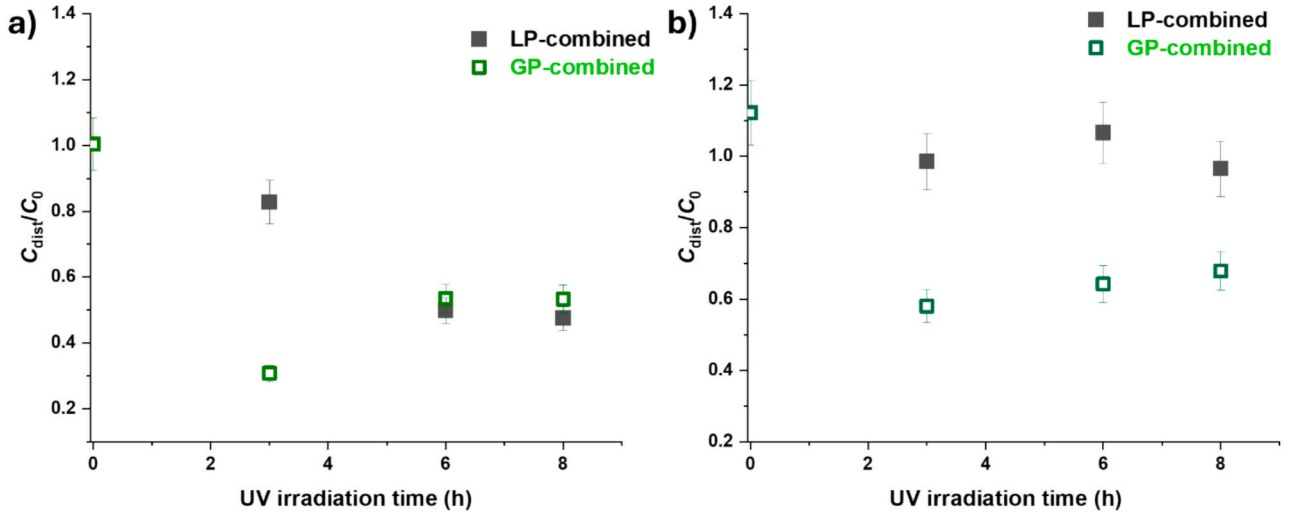

Fig. 5. Comparison of LP- and GP-combined tests performance (in terms of phenol concentration in the distillate, C_{dist}, normalized for the starting phenol concentration, C_0) carried out on a single pollutant solution in ultrapure water (a) and in simulated seawater (b).

Table 3
Synergy score, *SS*, for hydroquinone and benzoquinone in combined tests in ultrapure water calculated according to Eq. (3).

Tests	UV irradiation time (h)	Synergy Score (*SS*)	
		Hydroquinone	Benzoquinone
LP-combined tests	6	0.27	−0.01
	8	0.31	−0.05
GP-combined tests	6	0.29	0.00
	8	0.44	0.02

from tests of mixed pollutants (Fig. S7): GP-combined tests exhibited much lower phenol accumulation in the distillate throughout the experiment compared to the LP-combined approach. This leads to *SI* values >> 1. This marked synergy can be related to the fact that the evaporation step promotes the vaporization of just the VOC component, which can then be effectively degraded by the photocatalyst, whereas the non-volatile interferents remain confined to the liquid phase.

As the photocatalytic degradation of aromatic pollutants in the gas phase can lead to deactivation of the photocatalyst by adsorption of non-volatile residues, the TiO_2 layer surface was analyzed via FTIR before and after usage in a GP-combined test. Results (Fig. S8) show no apparent accumulation of organic residues at the surface. Moreover, consecutive tests were carried out on the same photocatalyst without any reactivation steps in between. Day–night cycles were simulated by 8 h of irradiation followed by 16 h in the dark. The results are reported in Fig. S9 and show no performance decrease after 56 h of operation. The presence of water vapor is known to promote the degradation of aromatic compounds in the gas phase, thereby limiting the formation of carbonaceous residues that can deactivate the photocatalyst surface. In this respect, the humid conditions within the solar still may be beneficial.

4. Conclusions

Photocatalytic photothermal evaporators are gaining traction as effective water purification systems capable of removing both inorganic and organic pollutants, and they hold promise as low-cost and low-energy desalination technologies. However, the interplay between the two processes remains poorly understood. In this study, we focused on the sequential application of photocatalysis and evaporation, demonstrating for the first time the potential for synergistic enhancements. These effects are not related to a specific combination of materials employed in the photocatalytic–photothermal evaporator, as they reflect the interplay between VOC oxidation by photocatalysis and pollutant rejection by evaporation, hence they hold potential to be of broad relevance. However, specific interactions between the photocatalyst and the photothermal catalyst were here not considered as they are highly system-specific and will require further dedicated investigations.

The synergistic action of photocatalysis and pollutant rejection by evaporation is reported here for the first time for degradation intermediates, particularly those arising from the attack of hydroxyl radicals on the aromatic ring. Since this is a very common degradation pathway in advanced oxidation processes, this finding has general significance. Moreover, we identified p-benzoquinone as an intermediate of particular concern due to its high volatility, which makes the combination of photocatalysis in the liquid phase and rejection by evaporation less effective for its removal.

Furthermore, we demonstrate here the critical role of the water matrix by discussing two key cases: widespread inorganic electrolytes and non-volatile organic compounds. Operating under these more challenging conditions can render the combination of photocatalysis and rejection by evaporation practically ineffective. To the authors' best knowledge, this is the first recognition of this issue for photocatalytic–photothermal evaporators. It is also worth noting that, while simulated seawater is commonly used for photothermal evaporation tests, photocatalytic tests for photocatalytic-photothermal evaporators are often carried out in water matrices with low salt content. As the sensitivity to electrolytes and specific reaction pathways can vary among photocatalysts, further studies in this direction are encouraged.

A better understanding of the interplay between photocatalysis and pollutant rejection by evaporation enabled us to design a more efficient strategy for combining the two approaches (GP-combined treatment). By bringing the evaporation step forward, some of the interfering effects of non-volatile species on photocatalysis are eliminated, resulting in a more efficient overall process. This leads to clear synergistic effects when treating complex water matrices, whereas the conventional combination of liquid-phase photocatalysis and pollutant rejection by evaporation is mostly additive in nature. It should be noted that, in the literature, most photocatalytic–photothermal evaporator devices rely predominantly on liquid-phase photocatalysis, and the role of photocatalysts exposed to the gas phase is often overlooked. Our study should open the door to the rational design of photocatalytic–photothermal systems that more effectively exploit gas-phase photocatalysis and optimized sequencing of the two processes.

CRediT authorship contribution statement

Hady Hamza: Writing – original draft, Visualization, Methodology, Investigation, Data curation. **Marco L.P. Schiavoni:** Methodology, Investigation. **Begüm Aksu:** Investigation. **Abdul Basit Shah Syed:** Writing – review & editing. **Vanni Lughi:** Writing – review & editing, Validation, Funding acquisition, Conceptualization. **Maria Vittoria Diamanti:** Writing – review & editing, Validation, Resources, Methodology, Funding acquisition. **Daniela Meroni:** Writing – original draft, Resources, Methodology, Funding acquisition, Data curation, Conceptualization.

Funding

This research was funded under the National Recovery and Resilience Plan (NRRP), Mission 4, Component 2, Investment 1.1, Call for tender No. 1409 published on 14.9.2022 by the Italian Ministry of University and Research (MUR), funded by the European Union – NextGenerationEU– Project Title COPE - COmposite nanomaterials coupling Photothermal Evaporation and photocatalysis for durable water purification systems – CUP G53D23006660001 - Grant Assignment Decree No. 1384 adopted on 01.09.2023 by the Italian Ministry of Ministry of University and Research (MUR).

Declaration of competing interest

The authors declare the following financial interests/personal relationships which may be considered as potential competing interests:

Daniela Meroni reports financial support was provided by ministero dell'università e della ricerca. If there are other authors, they declare that they have no known competing financial interests or personal relationships that could have appeared to influence the work reported in this paper.

Appendix A. Supplementary data

Supplementary data to this article can be found online at https://doi.org/10.1016/j.cej.2026.174182.

Data availability

Research data are available at the following https://zenodo.org/records/18676124.

References

[1] FAO, The State of Food and Agriculture 2020. Overcoming Water Challenges in Agriculture. Rome, 2020, https://doi.org/10.4060/cb1447en.
[2] E. Jones, M. Qadir, M.T.H. van Vliet, V. Smakhtin, S.-M. Kang, The state of desalination and brine production: a global outlook, Sci. Total Environ. 657 (2019) 1343–1356, https://doi.org/10.1016/j.scitotenv.2018.12.076.
[3] K. Elsaid, M. Kamil, E.T. Sayed, M.A. Abdelkareem, T. Wilberforce, A. Olabi, Environmental impact of desalination technologies: a review, Sci. Total Environ. 748 (2020) 141528, https://doi.org/10.1016/j.scitotenv.2020.141528.
[4] C. Song, W. Pi, P. Li, W. Liu, Water-first, energy-second: water management strategies propelling solar-driven interfacial water evaporation beyond limits, J. Environ. Chem. Eng. 13 (2025) 119183, https://doi.org/10.1016/j.jece.2025.119183.
[5] P. Tao, G. Ni, C. Song, W. Shang, J. Wu, J. Zhu, G. Chen, T. Deng, Solar-driven interfacial evaporation, Nat. Energy 3 (2018) 1031–1041, https://doi.org/10.1038/s41560-018-0260-7.
[6] X. Wu, Y. Lu, X. Ren, P. Wu, D. Chu, X. Yang, H. Xu, Interfacial solar evaporation: from fundamental research to applications, Adv. Mater. 36 (2024) 2313090, https://doi.org/10.1002/adma.202313090.
[7] X. Li, W. Xie, J. Zhu, Interfacial solar steam/vapor generation for heating and cooling, Adv. Sci. 9 (2022) 2104181, https://doi.org/10.1002/advs.202104181.
[8] V. Fthenakis, P. Xu, Z. Zhang, K. Sitterley, A. Lugo, H. Wang, S. Kuravi, K. Kota, N. Dani, A. Atia, Review of solar-enabled desalination and implications for zero-liquid-discharge applications, Progress Energy 6 (2024) 032004, https://doi.org/10.1088/2516-1083/ad43aa.
[9] Z. Zhu, Y. Xu, Y. Luo, W. Wang, X. Chen, Porous evaporators with special wettability for low-grade heat-driven water desalination, J. Mater. Chem. A 9 (2021) 702–726, https://doi.org/10.1039/D0TA09193F.
[10] H.T. Kim, L. Philip, A. McDonagh, M. Johir, J. Ren, H.K. Shon, L.D. Tijing, Recent advances in high-rate solar-driven interfacial evaporation, Adv. Sci. 11 (2024) 2401322, https://doi.org/10.1002/advs.202401322.
[11] L. Zhang, X. Li, Y. Zhong, A. Leroy, Z. Xu, L. Zhao, E.N. Wang, Highly efficient and salt rejecting solar evaporation via a wick-free confined water layer, Nat. Commun. 13 (2022) 849, https://doi.org/10.1038/s41467-022-28457-8.
[12] F. Zhao, X. Zhou, Y. Shi, X. Qian, M. Alexander, X. Zhao, S. Mendez, R. Yang, L. Qu, G. Yu, Highly efficient solar vapour generation via hierarchically nanostructured gels, Nat. Nanotechnol. 13 (2018) 489–495, https://doi.org/10.1038/s41565-018-0097-z.
[13] R. Chen, T. Zhang, J. Kim, H. Peng, M. Ye, C.-H. Huang, Interfacial solar distillation for freshwater production: fate of volatile and semivolatile organic contaminants, Environ. Sci. Technol. 55 (2021) 6248–6256, https://doi.org/10.1021/acs.est.0c07191.
[14] R. Djellabi, L. Noureen, V.-D. Dao, D. Meroni, E. Falletta, D.D. Dionysiou, C. L. Bianchi, Recent advances and challenges of emerging solar-driven steam and the contribution of photocatalytic effect, Chem. Eng. J. 431 (2022) 134024, https://doi.org/10.1016/j.cej.2021.134024.
[15] D.B. Miklos, C. Remy, M. Jekel, K.G. Linden, J.E. Drewes, U. Hübner, Evaluation of advanced oxidation processes for water and wastewater treatment – a critical review, Water Res. 139 (2018) 118–131, https://doi.org/10.1016/j.watres.2018.03.042.
[16] I. Michael, L. Rizzo, C.S. McArdell, C.M. Manaia, C. Merlin, T. Schwartz, C. Dagot, D. Fatta-Kassinos, Urban wastewater treatment plants as hotspots for the release of antibiotics in the environment: a review, Water Res. 47 (2013) 957–995, https://doi.org/10.1016/j.watres.2012.11.027.
[17] P. Zhang, H. Wang, J. Wang, Z. Ji, L. Qu, Boosting the viable water harvesting in solar vapor generation: from interfacial engineering to devices design, Adv. Mater. 36 (2024) 2303976, https://doi.org/10.1002/adma.202303976.
[18] S. Yan, H. Song, Y. Li, J. Yang, X. Jia, S. Wang, X. Yang, Integrated reduced graphene oxide/polypyrrole hybrid aerogels for simultaneous photocatalytic decontamination and water evaporation, Appl. Catal. B Environ. 301 (2022) 120820, https://doi.org/10.1016/j.apcatb.2021.120820.
[19] J. Ma, L. An, D. Liu, J. Yao, D. Qi, H. Xu, C. Song, F. Cui, X. Chen, J. Ma, W. Wang, A light-permeable solar evaporator with three-dimensional photocatalytic sites to boost volatile-organic-compound rejection for water purification, Environ. Sci. Technol. 56 (2022) 9797–9805, https://doi.org/10.1021/acs.est.2c01874.
[20] J.-L. Wu, L. Xu, S.-J. Han, L. Labiadh, M.-L. Fu, B. Yuan, Manganese oxide hydrogel for efficient removal of volatile organic compound in the photothermal water purification, Sol. RRL 8 (2024) 2300971, https://doi.org/10.1002/solr.202300971.
[21] H. Hamza, M.V. Diamanti, V. Lughi, S. Rossi, D. Meroni, Design efficiency: a critical perspective on testing methods for solar-driven Photothermal evaporation and photocatalysis, Nanomat 15 (2025) 1121, https://doi.org/10.3390/nano15141121.
[22] L. Rimoldi, D. Meroni, E. Falletta, V. Pifferi, L. Falciola, G. Cappelletti, S. Ardizzone, Emerging pollutant mixture mineralization by TiO_2 photocatalysts. The role of the water medium, Photochem. Photobiol. Sci. 16 (2017) 60–66, https://doi.org/10.1039/C6PP00214E.
[23] N. Rioja, S. Zorita, F.J. Peñas, Effect of water matrix on photocatalytic degradation and general kinetic modeling, Appl. Catal. B Environ. 180 (2016) 330–335.
[24] C. Lin, K.-S. Lin, Photocatalytic oxidation of toxic organohalides with TiO_2/UV: the effects of humic substances and organic mixtures, Chemosphere 66 (2007) 1872–1877, https://doi.org/10.1016/j.chemosphere.2006.08.027.
[25] S. Tang, L. Xu, X. Yu, S. Chen, H. Li, Y. Huang, J. Niu, Degradation of anticancer drug capecitabine in aquatic media by three advanced oxidation processes: mechanisms, toxicity changes and energy cost evaluation, Chem. Eng. J. 413 (2021) 127489, https://doi.org/10.1016/j.cej.2020.127489.
[26] D. Meroni, M. Jimenez-Salcedo, E. Falletta, B.M. Bresolin, C.F. Kait, D.C. Boffito, C. L. Bianchi, C. Pirola, Sonophotocatalytic degradation of sodium diclofenac using low power ultrasound and micro sized TiO_2, Ultrason. Sonochem. 67 (2020) 105123, https://doi.org/10.1016/j.ultsonch.2020.105123.
[27] A. Santos, P. Yustos, A. Quintanilla, F. García-Ochoa, J.A. Casas, J.J. Rodríguez, Evolution of toxicity upon wet catalytic oxidation of phenol, Environ. Sci. Technol. 38 (2004) 133–138, https://doi.org/10.1021/es030476t.
[28] F.J. Enguita, A.L. Leitão, Hydroquinone: environmental pollution, toxicity, and microbial answers, Biomed. Res. Int. 2013 (2013) 1–14, https://doi.org/10.1155/2013/542168.
[29] M.V. Diamanti, M.V. Shinnur, M. Pedeferri, A.M. Ferrari, R. Rosa, D. Meroni, Toward sustainable photocatalysis: addressing deactivation and environmental impact of anodized and sol–gel photocatalysts, Adv. Sustainable Syst. 9 (2025) 2401017, https://doi.org/10.1002/adsu.202401017.
[30] M. Sheng, Y. Yang, X. Bin, S. Zhao, C. Pan, F. Nawaz, W. Que, Recent advanced self-propelling salt-blocking technologies for passive solar-driven interfacial evaporation desalination systems, Nano Energy 89 (2021) 106468, https://doi.org/10.1016/j.nanoen.2021.106468.
[31] B. Chaw Pattnayak, S. Mohapatra, Photothermal-photocatalytic CSG@ZFG evaporator for synergistic salt rejection and VOC removal during solar-driven water distillation, Langmuir 39 (2023) 4651–4661, https://doi.org/10.1021/acs.langmuir.2c03438.
[32] H. Sopha, A. Kashimbetova, L. Hromadko, I. Saldan, L. Celko, E.B. Montufar, et al., Anodic TiO_2 nanotubes on 3D-printed titanium meshes for photocatalytic

applications, Nano Lett. 21 (2021) 8701–8706, https://doi.org/10.1021/acs.nanolett.1c02815.
[33] A. Sobczyński, Ł. Duczmal, W. Zmudziński, Phenol destruction by photocatalysis on TiO2: an attempt to solve the reaction mechanism, J. Mol. Catal. A Chem. 213 (2004) 225–230, https://doi.org/10.1016/j.molcata.2003.12.006.
[34] T.T.T. Dang, S.T.T. Le, D. Channei, W. Khanitchaidecha, A. Nakaruk, Photodegradation mechanisms of phenol in the photocatalytic process, Res. Chem. Intermed. 42 (2016) 5674–5961, https://doi.org/10.1007/s11164-015-2417-3.
[35] L. Suhadolnik, A. Pohar, B. Likozar, M. Čeh, Mechanism and kinetics of phenol photocatalytic, electrocatalytic and photoelectrocatalytic degradation in a TiO2-nanotube fixed-bed microreactor, Chem. Eng. J. 303 (2016) 292–301, https://doi.org/10.1016/j.cej.2016.06.027.
[36] J. Zhang, G. Zhang, H. Lan, M. Sun, H. Liu, J. Qu, Synergetic oxidation of the hydroxyl radical and superoxide anion lowers the benzoquinone intermediate conversion barrier and potentiates effective aromatic pollutant mineralization, Environ. Sci. Technol. 57 (2023) 12117–12126, https://doi.org/10.1021/acs.est.3c03406.
[37] Jung Jung, Y. Soo, B. Oh, J.-W. Kang, Synergistic effect of sequential or combined use of ozone and UV radiation for the disinfection of *Bacillus subtilis* spores, Water Res. 42 (2008) 1613–1621, https://doi.org/10.1016/j.watres.2007.10.008.
[38] E. Pino, M.V. Encinas, Photocatalytic degradation of chlorophenols on TiO_2-325 mesh and TiO_2-P25. An extended kinetic study of photodegradation under competitive conditions, J. Photochem. Photobiol. A Chem. 242 (2012) 20–27, https://doi.org/10.1016/j.jphotochem.2012.05.019.